



## Determination of Convective Heat Transfer Coefficients Using 2D MRI Temperature Mapping and Finite Element Modeling

Greg J. Hulbert,<sup>a,b,\*</sup> J. Bruce Litchfield<sup>c</sup> & Shelly J. Schmidt<sup>d</sup>

<sup>a</sup>Department of Food Science and Technology, University of Tennessee, Knoxville, TN 37901, USA

<sup>b</sup>Department of Agricultural Engineering, University of Tennessee, Knoxville, TN 37901, USA

<sup>c</sup>Department of Agricultural Engineering, University of Illinois, Urbana, IL 61801, USA

<sup>d</sup>Department of Food Science and Human Nutrition, University of Illinois, Urbana, IL 61801, USA

(Received 24 October 1995; revised 27 May 1997; accepted 10 June 1997)

### ABSTRACT

*Finite element modeling was used in combination with 2D MRI temperature mapping to calculate fluid to particle convective heat transfer coefficients ( $h_{fp}$ ) across the surfaces of a carrot particle being heated with 80°C water with an average velocity of 4.4 cm/s. Heat transfer in the region of interest (image acquired from center of sample) was essentially two-dimensional because of the length of the carrot sliver. The  $h_{fp}$  at each surface was determined by trial and error matching of temperature contours in the model to those in the MRI image. Calculated values of  $h_{fp}$  (117–389 W/m<sup>2</sup> K) were within the range of those reported in the literature. The major advantages of this method are that the actual shape of the food particle is used in the model, and it can be utilized in applications where the particle does not heat uniformly from all directions.*  
© 1998 Elsevier Science Limited. All rights reserved

### INTRODUCTION

In an aseptic processing system for a fluid food containing particulates, two phases of heat transfer occur simultaneously. External heat is applied to the fluid rapidly increasing the temperature, and as the fluid temperature rises, heat is transferred to the particles. The rate of this convective heat transfer is a function of the physical

\*Author to whom all correspondence should be addressed.

properties of the particle surface, the rheological properties of the fluid, and the relative motion of particle and fluid. The overall effect of these components is accounted for with the fluid to particle convective heat transfer coefficient ( $h_{fp}$ ). Values for  $h_{fp}$  are very difficult to determine. Empirically determined formulas are available (de Ruyter & Brunet, 1973; Deniston *et al.*, 1987) for applications involving regularly shaped particles (spheres, cubes, etc.) with predictable flow patterns (relative velocity known). However, with aseptic processing systems the relative velocity is variable and difficult to determine.

In a previous work (Hulbert *et al.*, 1995)  $T_1$ -weighted NMR imaging was reported as a means to map temperature distributions in particulates during heating. A review of related studies involving medical applications is also reported there. Using this technique with faster scan times could allow measurement of particulate cold point temperatures in a flowing system. In addition, measurement of heat transfer coefficients could aid in the design and model validation of aseptic systems.

The objective of this study was to demonstrate the value of MRI temperature mapping for use in modeling applications in which temperature contours are difficult to predict. Doran *et al.* (1994) compared a finite element model to 2D MRI temperature maps in a polymer block, but the temperature contours were easy to predict and were measured at steady state. In our study, a trial and error modeling procedure was used to match temperature contours with those measured with MRI. Such a trial and error procedure (demonstrated here in principle) will be very useful for aseptic processing applications if the scan times are able to be reduced to the order of milliseconds.

## THEORY

The theory and mathematics for calculating temperature maps from  $T_1$ -weighted MRI images have been thoroughly discussed (Hulbert *et al.*, 1995). In that work the  $T_1$  temperature dependence between 20°C and 80°C for processed carrot was determined:

$$T_1 = 0.480 \text{ sec} + 0.0318 \text{ sec}/^\circ\text{C} \quad (1)$$

Signal intensity for the two-dimensional Fourier transform spin echo imaging sequence used is a function of  $T_1$  and a proportionality factor  $\kappa(T)$  based on the Boltzmann distribution:

$$S = \kappa(T)\rho [1 - e^{-T_R/T_1}] \quad (2)$$

Because both  $T_1$  and  $\kappa(T)$  are temperature dependent an iterative solution procedure is required. The repetition time ( $T_R$ ) is strategically set by the experimental operator for optimal temperature sensitivity. For a sample with a length-to-width ratio  $> 5.0$ , heat transfer at the center can be assumed to be two-dimensional. That is, the heating from the ends of the sample is neglected. The governing differential equation for this problem is

$$\rho C_p \frac{\partial T}{\partial t} = \frac{\partial}{\partial x} \left( k_x \frac{\partial T}{\partial x} \right) + \frac{\partial}{\partial y} \left( k_y \frac{\partial T}{\partial y} \right) \quad (3)$$

where  $\rho$  is the density,  $C_p$  is the specific heat, and  $k$  is the thermal conductivity. When the thermal conductivity is constant along both the  $x$  and  $y$  axes, then eqn (3) reduces to

$$\frac{1}{\alpha} \frac{\partial T}{\partial t} = \frac{\partial^2 T}{\partial x^2} + \frac{\partial^2 T}{\partial y^2} \quad (4)$$

where  $\alpha$  is the thermal diffusivity. This is Poisson's equation with temperature as the primary unknown. It can be used as the basis for the following matrix equation:

$$[C]\{\dot{T}\} + [K]\{T\} = 0 \quad (5)$$

where  $[C]$  is the specific heat matrix,  $[K]$  is the thermal conductivity matrix (including equivalent face convection terms), and  $\{T\}$  is the node temperature vector. The transposed node temperature and time derivative node temperature vectors are

$$\{T\}^T = [T_1 \ T_2 \ \dots \ T_n] \quad (6)$$

and

$$\{\dot{T}\}^T = \left[ \frac{\partial T_1}{\partial t} \quad \frac{\partial T_2}{\partial t} \quad \dots \quad \frac{\partial T_n}{\partial t} \right] \quad (7)$$

## MATERIALS AND METHODS

### NMR imaging

Images were acquired with a two-dimensional Fourier transform (2DFT) spin echo pulse sequence (Hahn, 1950). It was modified to allow use of the shortest possible  $T_E$  so that  $T_1$ -weighting would be maximized. A 200 MHz, 4.7 T (tesla) imager was used at the Biomedical Magnetic Resonance Laboratory at the University of Illinois. The saddle coil probe was 4 cm in diameter and the radio frequency coil region was 8 cm long. Images were processed with image-processing software Viewit (1991).

The MRI sampling parameters were  $T_R = 0.74$  s,  $T_E = 17$  ms,  $\Delta Z = 0.47$  cm,  $D_x = 3$  cm,  $D_y = 1$  cm,  $N_x = 128$ , and  $N_y = 16$ ; where  $T_R$  was the repetition time,  $T_E$  was the echo delay time,  $\Delta z$  was the image slice thickness,  $D_x$  was the field of view in the frequency encoding direction,  $D_y$  was the field of view in the phase encoding direction,  $N_x$  was the number of frequency encodes, and  $N_y$  was the number of phase encodes. Therefore, the sampling resolution was 0.234 mm in the frequency encoding direction and 0.625 mm in the phase encoding direction. Images were stretched in the phase encoding direction so that each dimension was 128 pixels long.

### Sample preparation and procedure

A sliver 5 cm long was cut with a knife from a section of a carrot outside of the core. It was cut such that the cross-section was polygonal in shape in order to create

**TABLE 1**  
Fluid to Particle Convective Heat Transfer Coefficients ( $h_{fp}$ ) Calculated by Finite Element Analysis

Surface	Length (mm)	$h_{fp}$ ( $W/m^2\text{°K}$ )
<i>a</i>	5.8	6
<i>b</i>	0.9	156
<i>c</i>	1.8	156
<i>d</i>	5.5	389
<i>e</i>	0.4	*
<i>f</i>	2.5	156
<i>g</i>	2.4	117
<i>h</i>	1.2	233
<i>i</i>	1.8	233
Literature values	–	55–350 <sup>a</sup> , 239–303 <sup>b</sup> , > 350 <sup>c</sup>

\*Heat transfer negligible compared to adjoining surfaces.

<sup>a</sup>Potato spheres heated with 68°C water (Califano and Calvelo, 1983).

<sup>b</sup>Sweet potato cubes heated with 132°C water (Chang and Toledo, 1989).

<sup>c</sup>Carrot cubes heated with 140°C water (Chang and Toledo, 1990).

different flow patterns of the heated water past the sample. Dimensions of the carrot cross-section are listed in Table 1. The sample was thoroughly cooked and was fixed within a plastic tube (7.5 mm i.d.) with a series of toothpick pieces. The cross-sectional area of the tube relative to the carrot was approximately 2:1, but one edge of the carrot was very close to the tube wall. The tube and sample were allowed to cool and were fixed in the center of the imaging probe. Insulated rubber tubing was connected to both ends of the sample tube, and the probe was centered within the imager (Fig. 1). Water from a constant temperature bath originally bypassed the sample until water in the bath and tubing reached 80°C. Three-way valves were then used to divert the flow through the sample tube, and the experiment was started when the water reached the sample tube 4 s later. The data acquisition time for each image was approximately 12 s. Therefore, each acquisition was started 6 s before the nominal sampling time.

## Modeling

ANSYS 5.0 (1993) was used to model the temperature distributions within the carrot particulates. The ANSYS stiffness matrix was Stiff-55 (two-dimensional thermal solid). A two-dimensional mesh with several hundred elements was created with an automatic mesh generation routine. The mesh boundaries were set to match the dimensions of the MRI image. Thermal conductivity values ( $k = 0.591 \pm 0.006$  W/m K) for processed carrots were measured by Murakami (unpublished data, 1993). Specific heat ( $C_p = 0.96$  cal/g °C) was calculated from the moisture content ( $C_p = 0.8M + 0.2$ ). The fluid to particle convective heat transfer coefficient ( $h_{fp}$ ) at each surface was determined by trial and error matching of heating profiles in the model to those determined with MRI measurements.

The matrix equation, eqn (5), was solved by an implicit direct integration scheme based on a modified Houbolt method. A quadratic temperature function

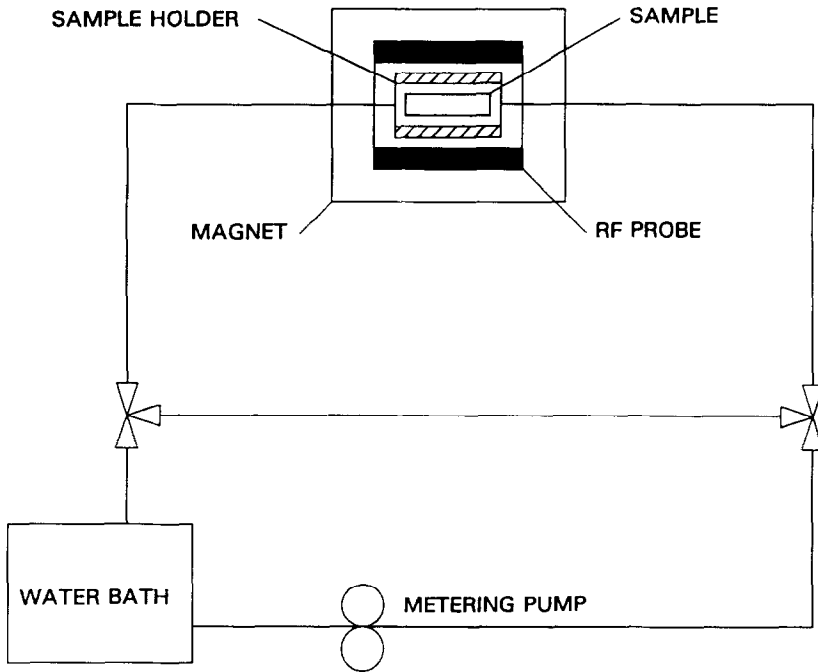


Fig. 1. Schematic of experimental apparatus.

$$T_i = a + bt + ct^2 \quad (8)$$

was differentiated and substituted into eqn (5) to yield an equation with three unknowns:  $a$ ,  $b$ , and  $c$ . With  $\Delta t$  being the time step between iterations, a set of three equations was defined at  $(t, t - \Delta t, t - 2\Delta t)$  and solved simultaneously to give the integration equation:

$$\left[ \frac{C_1}{\Delta T} [C] + [K] \right] \{T_i\} = f([C], \{T_{t-\Delta t}\}, \{T_{t-2\Delta t}\}) \quad (9)$$

This equation was solved for  $T_i$  based on the solutions at the previous times. The integration time step  $\Delta t$  was chosen on the basis of the 'conducting length' of the element. The larger the thermal gradient to be resolved, the smaller both the element length and the integration time step. The initial  $\Delta t$  was selected using the relationship  $\Delta t_i \approx \delta^2 / (4\alpha)$ . In this relationship  $\alpha$  is the material thermal diffusivity, and  $\delta$  is the conducting length of an element in the region over which the largest gradient acts (usually the length parallel to the heat flow direction of the element adjacent to the surface). However, if  $\Delta t$  is too small, temperature oscillations may occur in the lower gradient regions. Abrupt changes in  $\Delta t$  between iterations are not recommended unless the temperature change is fairly linear. A time step optimization procedure was used to allow the most efficient use of CPU time.

## RESULTS AND DISCUSSION

The finite element mesh for the model is shown in Fig. 2. The model had nine sides or surfaces which were labeled with lower case letters. Surface 'a' was in contact with the wall of the tube containing the sample so there was only a slight flow of heating water past that surface and, therefore, little heat transfer. Heat transfer across the other surfaces of the carrot varied according to the local flow patterns of the water past each surface. The fluid to particle convective heat transfer coefficient  $h_{fp}$  at each surface was used as the load step or final boundary condition to solve the problem. The relative values for  $h_{fp}$  were determined by trial and error by matching the temperature contours of the model to those in the MRI image (Fig. 3). The temperature contours did not change with time but only the magnitude of the temperatures. Therefore, any or all images can be used for this trial and error procedure. Because the procedure uses essentially all the data points, the measure-

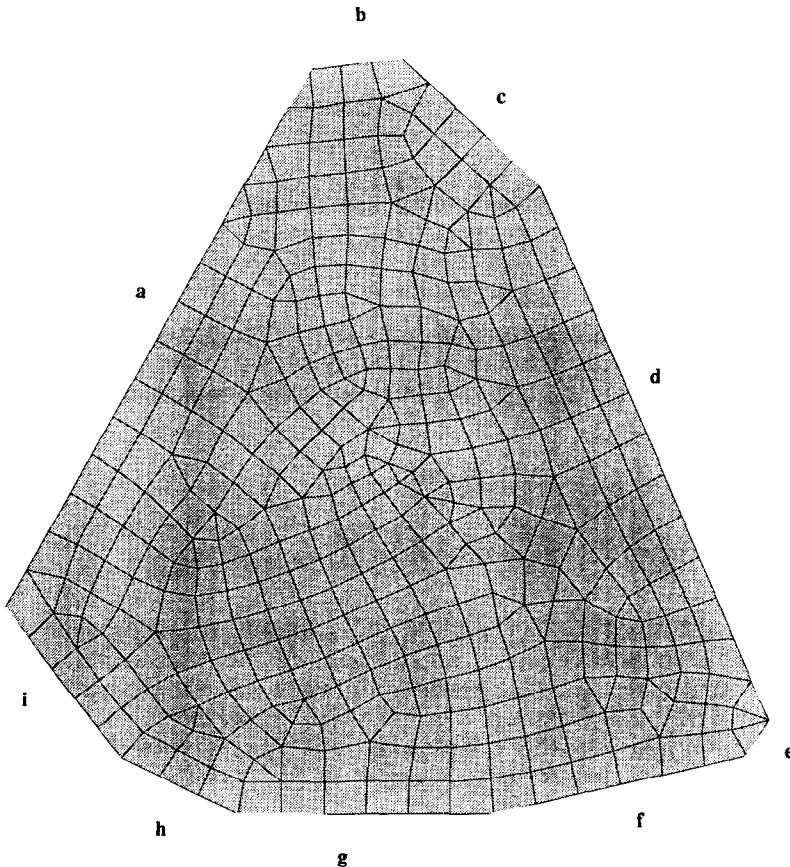


**Fig. 2.** Finite element mesh generated to match the dimensions of the cross-sectional carrot slice. The dimensions of the surfaces designated with lower case letters are listed in Table 1.

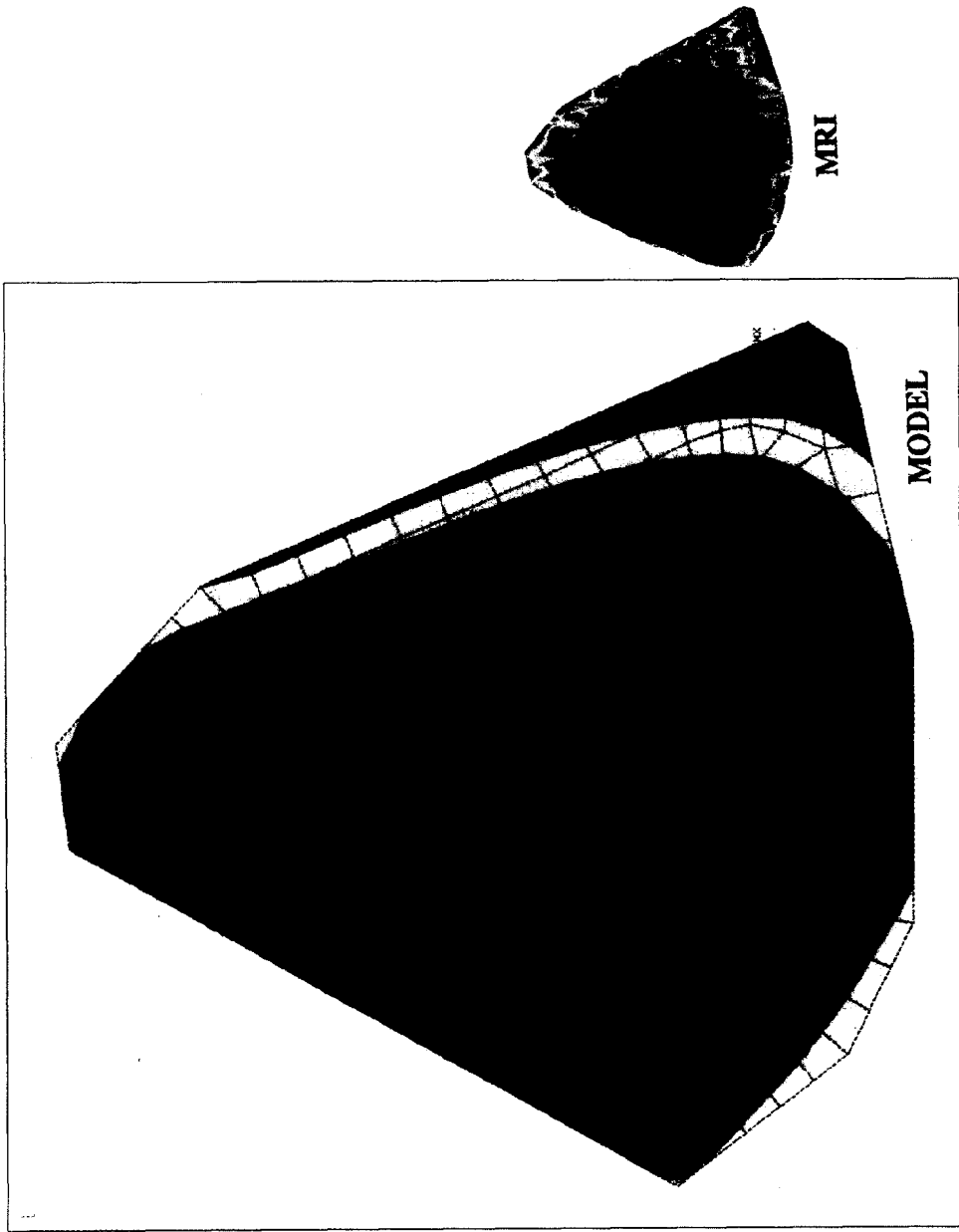
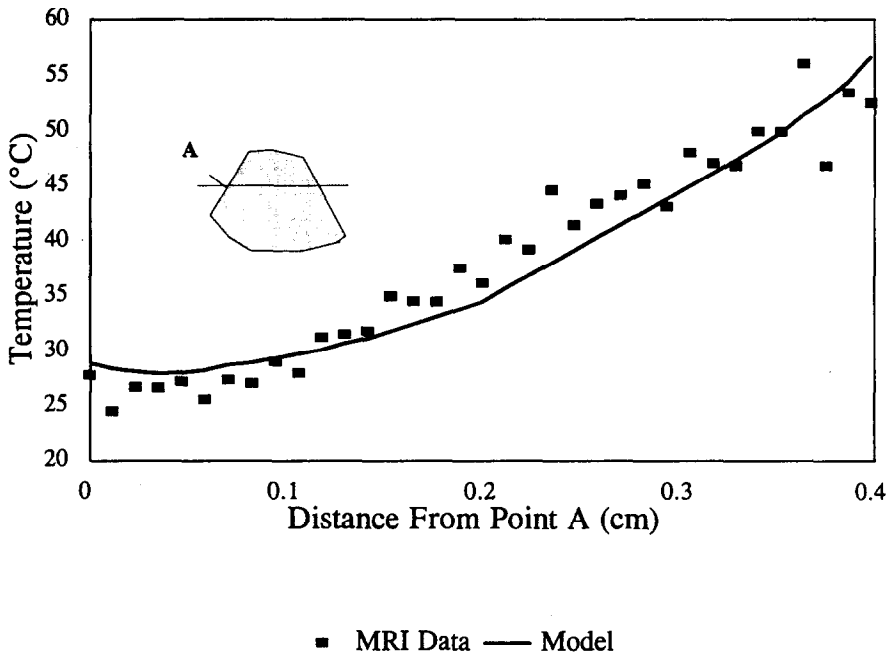


Fig. 3. Temperature contours in the finite element model were matched to those of the MRI temperature map. This yielded the relative values of  $h_{fp}$ . True  $h_{fp}$  values were determined by comparison of actual temperature values as in Fig. 4. The carrot sliver was heated with 80°C water for 20 s.

ment error for relative values of  $h_{fp}$  is greatly reduced compared to the error of local temperature values. This is due to the fact that the measurement noise (radio frequency noise) is randomly distributed throughout the sample, and the error due to this noise is drastically reduced by signal averaging (Hulbert *et al.*, 1995). However, this in effect only determined the normalized value of  $h_{fp}$  in relation to the other eight surfaces. The magnitude of the  $h_{fp}$  values was determined by comparison of temperature magnitudes measured by MRI to the model. This was accomplished by taking a horizontal profile through the image and converting signal intensity to temperature using eqn (1). A profile of temperatures at the same location was calculated by the model and plotted versus the MRI data (Fig. 4). The values for  $h_{fp}$  (Table 1) were within the range of those reported in the literature for experiments with low fluid velocities (Califano & Calvelo, 1983; Chang & Toledo, 1989). Chang and Toledo (1990) calculated higher heat transfer coefficients for carrot cubes heated in water. However, the water temperature in their study was 140°C, and therefore the fluid viscosity was lower. Also,  $h_{fp}$  is highly dependent on fluid velocity and particle size and shape.

This method could be useful in confirming heat transfer models for foods of irregular shape or where the fluid flow is not uniform around the sample. In these cases cold point location and heat transfer patterns are unpredictable, and therefore modeling based on thermocouple readings is not practical. A temperature map is much more useful than limited number of point source temperatures, especially in



**Fig. 4.** Temperature values from the finite element model were compared to those obtained with MRI. The comparison was made for a horizontal profile through the image beginning at point A. This was a trial and error procedure that yielded the calculated values of  $h_{fp}$  at each surface (Table 1).

determining relative values of  $h_{fp}$  and/or locating the cold point of the sample. Also thermocouples are invasive and restrict the flow of the particles. Reduction in MRI temperature mapping scan times would allow the experimental error (due to temperature changes during data acquisition) to be reduced.

There was considerable scatter in the local MRI temperature data (Fig. 4), but normalized values of  $h_{fp}$  were not affected by this measurement noise. The actual magnitude of  $h_{fp}$  values was significantly affected by the experimental error of the technique, but this is primarily due to the influence of scan time. Image processing procedures are being developed to allow faster scan times and at the same time reduce scatter caused by measurement noise (Hulbert, 1994). However, even with the scan time used in this study, the technique is useful in determining normalized or relative values of  $h_{fp}$ .

This method could also be improved with the incorporation of more detailed thermal property data. For instance, the temperature dependence of thermal conductivity values is easily incorporated into the finite element model. Although the reported data was based on one replication, temperature maps were acquired at various time intervals. Normalized  $h_{fp}$  values were based on temperature contours the shape of which were the same at each time interval. The resolution of the contours was the greatest at the shortest heating time because of the magnitude of the temperature gradients.

## REFERENCES

- ANSYS 5.0 (1993). *Engineering Analysis System Users Manual* by G. J. Desalvo and R. W. Gorman. Swanson Analysis Systems, Houston, PA.
- Califano, A. N. & Calvelo, A. (1983). Heat and mass transfer during the warm water blanching of potatoes. *J. Food Sci.*, **48**, 220–225.
- Chang, S. Y. & Toledo, R. T. (1989). Heat transfer and simulated sterilization of particulate solids in a continuously flowing system. *J. Food Sci.*, **54**, 1017–1023.
- Chang, S. Y. & Toledo, R. T. (1990). Simultaneous determination of thermal diffusivity and heat transfer coefficient during sterilization of carrot dices in a packed bed. *J. Fluid Sci.*, **55**, 199–205.
- Deniston, M. F., Hassan, B. H. & Merson, R. L. (1987). Heat transfer coefficients to liquid with food particles in axially rotating cans. *J. Food Sci.*, **56**(4), 962
- de Ruyter, P. W. & Brunet, R. (1973). Estimation of process conditions for continuous sterilization of foods containing particles. *Food Technol.*, **27**(7), 44
- Doran, S. J., Carpenter, T. A. & Hall, L. D. (1994). Noninvasive measurement of temperature distributions with high spatial resolution using quantitative imaging of NMR relaxation times. *Rev. Sci. Instrum.*, **65**(7), 2231–2237.
- Hahn, E. L. (1950). Spin echoes. *Phys. Rev.*, **80**, 580–594.
- Hulbert, G. J. (1994). MRI temperature mapping and finite element modeling of heat transfer in carrot particulates undergoing thermal processing. Ph.D. thesis, University of Illinois, Urbana, IL.
- Hulbert, G. J., Litchfield, J. B. & Schmidt, S. J. (1995). Temperature mapping in a carrot using  $T_1$  weighted magnetic resonance imaging. *J. Food Sci.*, **60**(4), 780–785.
- Viewit (1991). Image processing software. Developed by Clint Potter, National Center for Supercomputer Applications and Biomedical Magnetic Resonance Laboratory, University of Illinois, Urbana, IL.